AIAA Aviation
16-20 June 2014, Atlanta, GA
7th AIAA Flow Control Conference

First Principles Based PID Control of Mixing Layer: Role of Inflow Perturbation Spectrum

Upender K. Kaul*
NASA Ames Research Center, USA.

The most amplified (fundamental) wave and its subharmonics trigger the instabilities of a mixing layer and its subsequent development. In the present work, an approach for controlling mixing layers[1] is extended to assess the role of amplitude, phase and number of subharmonics of the most amplified wave. In the earlier study[1], a Proportional-Integral-Derivative (PID) control technique applied to a spectral solution was shown to be capable of rapidly driving the time-developing mixing layer to a target layer thickness, using the phase shift between the fundamental and its subharmonics as the control parameter. The present study uses the PID control technique with amplitude of the fundamental as the control variable to control the thickness of the mixing layer. The PID control demonstrates control of such layers by selectively picking and modulating the amplitude or relative phases of various modes. The previous study[1] demonstrated that an assessment of the control regime in the temporally developing mixing layer is sufficient for defining the perturbation envelope for controlling the spatially developing layer. This affords us an efficient way of defining the spectrum of perturbations that can lead to varying degree of instability of the spatially growing layer. Hence a variety of different perturbations have been studied in the temporal domain to assess their effect on the development of the layer. Simulations of spatially growing layer are also performed to support the conclusions. Additionally, a collective interaction study of spatially growing layer where various modes yield not just pairing of structures but a collective interaction of more than two structures at a time, has been carried out that results in an appreciable change in the growth rate of the layer.

Keywords: Free Shear Layer, Mixing Layer, Flow Control, PID Control, Stability Theory, Perturbation Spectrum.

1 Introduction

Free shear layers or mixing layers have been the subject of intense study for quite some time now[2], since they are present in a host of applications and present an excellent canonical problem for study. Sufficient knowledge has been gained from these studies to enable us to formulate strategies for their control. It may be desired to control the flow[3] to achieve a certain objective. For instance, the goal might be to increase mixing in the shear layer in a combustor to enhance mixing[4,5] or downstream of a jet[6–8], to reduce the sound emitted by a jet exhaust, to reduce resonance in the flow over a cavity[9–13], or to reduce the length of a separation bubble in the flow over an airfoil or turbine blade[14], or to reduce the drag of a bluff body[15,16].

In these applications, the incoming shear layer can be laminar or turbulent. In the present work, we consider inflow base profile described by an error function along with superimposed perturbations calculated from the linear inviscid theory. The error function profile is typical of free shear flows. In earlier work[1] as well as the present work, the mixing layer is forced using inviscid instability eigenfunctions.

* Applied Modeling and Simulations Branch, NASA Advanced Supercomputing (NAS) Division; Associate Fellow, AIAA

This paper reports results in continuation of a previous study[1], where it was shown that DNS of a spatially growing free shear (mixing) layer can be performed sufficiently accurately using boundary conditions mapped[17,18] from a time-developing, i.e., streamwise periodic simulation. Earlier PID control results[1] using phase shift as the control parameter are shown in Fig. 1. The phase shift between different harmonics was sought that leads to a target thickness of the layer at $x/\lambda_f = 2.5$, where λ_f is the wave length of the fundamental. This location marks the end of the linear development of the layer and hence is an appropriate location for the PID control which is a linear control algorithm. In the present study, the phase shifts are fixed and the amplitude of the fundamental is used as the control parameter, with the amplitudes of the subharmonics fixed by a given ratio to the amplitude of the fundamental. In one instance, the amplitude of the fundamental is fixed, and the amplitudes of the subharmonics are changed with respect to the fundamental. The ordinate in Fig. 1 represents the error, measured by the difference between the set point, target mixing layer thickness, δ_{target}, and the iterated layer thickness, δ, and the abcissa represents the phase shift. The PID control loop that drives the control algorithm is shown in Fig. 2. The error, $e(t)$, is the absolute value of the difference between the target shear layer thickness and the iterated shear layer thickness, $A(t)$ is the control output given by the PID control as an updated amplitude of the fundamental perturbation and $\delta(t)$ is the iterated shear layer thickness. For a time level corresponding to the nth PID iterate, $t = t_0 + (n-1)\epsilon$, where ϵ is the time taken by the CFD plant for each PID iteration and t_0 is some reference time, the following expression is calculated

$$\sum(t) = K_P e(t) + K_I \int_{t_0}^{t} e(\tau)d\tau + K_D de(t)/dt$$

where $e(t) = \delta^n$ - δ_{target}, and $\sum(t)$ denotes the sum of the proportional, integral and derivative components of the PID control loop at time, t. It is assumed here that the PID loop takes infinitesimally small amount of time outside of the CFD plant. Thus, the new amplitude, $A^n = A^{n-1} + \sum(t)$. The gain coefficients are chosen initially by trial and are reduced as the iterations converge.

2 Results

2.1 Mixing Layer with a Velocity Ratio, r= 0.5

The role of perturbations imposed near the origin of a two-dimensional free shear layer with a velocity ratio, r (u_{top}/u_{bottom}) = 0.5 will be discussed in the following paragraphs. This choice of velocity gives $\Delta u/u_m$ = 0.66, where $\Delta u = 2$ and $u_m = 3$. The unit of velocity is half of the shear across the layer. The initial velocity profile is an error function, superposed on which are eigenfunctions from the linear inviscid stability theory corresponding to various unstable modes. The Reynolds number based on the initial shear layer thickness is 50. Many experimental investigations[19–23] have been carried out at or around this velocity ratio. This allows us to compare experimental data with the present direct numerical simulation (DNS) results. The experimental data[19] show that there is a distinct difference in spreading rate and velocity profiles between the forced and the unforced mixing layer. Further, the effect of initial conditions has a lasting effect on the development of the mixing layer[19]. In another experimental study[20], the development of large eddies in the turbulent mixing layer have been observed to be governed by an inviscid instability at fairly large Re. As a matter of fact, mixing layer has been observed[24] to be turbulent at moderate Reynolds number. In free shear layer flow, stability of disturbances calculated from the linear theory has been shown[25] to be independent of Re beyond the value of 50, based on the initial shear layer thickness. Much of the experimental evidence points to the fact that the dynamics of the large scale structures in a mixing layer is predominantly two-dimensional, and that the entrainment of fluids into the mixing layer from outside is determined by these large structures[26]. It is this initial two-dimensional region of the mixing layer that we seek to control.

2.1.1 Influence of Relative Amplitudes of Different Harmonics

Various cases were studied where forcing levels of fundamental and its subharmonics were varied within the constraints of the linear theory, especially that of the fundamental. This is achieved by limiting the amplitude of the perturbation vertical velocity, v', at the midplane, $y = 0$, to be less than 1 percent of the unit velocity.

A revealing finding was made during this study that the amplitudes of the subharmonics can be prescribed at levels outside of the linear range, since they tend to remain dormant during the initial linear development of the layer, especially third and higher subharmonics of the fundamental. Progressively higher forcing levels can be imposed initially for higher subharmonics. This gives us a broad control regime to control the subsequent development of the layer in a rigorous tractable fashion. However, in practice, an actuator can provide forcing at higher levels that does not obey the linear limit. An investigation is currently underway that runs simulations[27−29] with initial conditions that match the experimental conditions[30,31]. In these DNS studies, velocity profiles (base flow + perturbation) will be extracted from the experimental data.

First, a comparison of profiles of momentum thickness, $\theta(t)$, and visual (streamline) thickness, $h(t)$ (also denoted by $\delta(t)$), is shown in Figs. 3(a) and 3(b), respectively, with three different forcing levels in the linear regime. Visual thickness is defined by the lateral extent of the largest closed instantaneous streamline, also known as the zero streamline, in the temporal domain. As the forcing level of the fundamental is increased from 0.9 percent to 4 percent, the growth rate of the layer increases. The growth rate of the mixing layer is defined by the average slope of the θ - time profile or the h - time profile. Next, fixing the fundamental wave forcing level at 0.9 percent and varying the forcing levels of the subharmonics, a larger growth rate of the layer is realized as shown through momentum thickness and visual thickness profiles in Fig. 4(a) and Fig. 4(b), respectively. When forcing levels of both subharmonics are increased to 4 times that of the fundamental, the largest growth rate is observed. When the forcing level of only the first subharmonic is increased, rate of growth is larger than when only the third subharmonic forcing level is increased; but, a larger lateral extent of the second paired structure is realized in the latter case, as expected. It turns out that the first subharmonic rather than the fundamental or the third subharmonic is most crucial in determining the growth rate of the layer. Due to recent advances in actuation such as provided by DBD actuators, it is now practical to provide actuation at individual frequencies, and hence a direct comparison between DNS and experiment can be made.

2.1.2 Influence of Relative Phase Shifts of Different Harmonics

The influence of relative phase shifts is most pronounced in determining the rate of growth of the layer. Fig. 5 shows that the phase shift of π between the subharmonics and the fundamental leads to dramatic suppression of the layer growth. The baseline, shown in magenta, being the case of zero phase shift, gives the largest growth rate of the layer at given forcing levels. The next best is the case of a phase shift of $\pi/4$, shown in blue. A phase shift of $\pi/2$ leads to a delayed growth of the layer with the first pairing substantially delayed. Fig. 6(a) shows that the phase shift between the fundamental and the first subharmonic is crucial in determining the growth rate of the layer. A phase shift of π between the fundamental and the first subharmonic leads to practically the same result as shown in Fig. 5 where both the subharmonics are shifted by π from the fundamental, once again highlighting the important role played by the first subharmonic. Fig. 6(b) shows results for the case where phase shift between the third subharmonic and the fundamental is considered. The results for a phase shift of $\pi/2$ are almost identical with those with the first subharmonic being out of phase by π with the fundamental, as expected, since the second subharmonic is an exact mutiple of the third subharmonic. Phase shift of π yields results identical to the baseline (phase shift equal to zero).

The effect of phase shift of both the first and the third subharmonics is more pronounced as shown in Figs. 7 and 8(a,b) via visual (streamline) thickness plots. Whereas the phase shift of $\pi/4$ yields results close to the baseline results, a phase shift of $\pi/2$ gives visual thickness markedly different from its momentum thickness counterpart, since the peak visual thickness is significantly below that corresponding to the baseline, unlike the momentum thickness peak which is greater than the baseline momentum thickness. Visual thickness evolution is similar to the momentum thickness evolution for phase shift of π. Again, there are differences in the visual thickness and momentum thickness profiles as shown in Fig. 8(a,b) and Fig. 6(a,b), the main difference being that the phase shift of π gives visual thickness markedly different from the baseline visual thickness.

2.1.3 Collective Interaction

So far we have discussed the mixing layer dynamics based on successive binary pairings of structures. The baseline case corresponds to zero phase shift of the three wave lengths and amplitudes, A_1=0.9 percent, $A_2 = A_3 = 0.5A_1$. We will consider this baseline case and introduce a fourth wave number into the

perturbation spectrum. This corresponds to the first fractional subharmonic of the fundamental, with three waves spanning four fundamental waves. A DNS of the spatially growing layer is performed using the EDLFLOW solver[27−29]. The EDLFLOW solver directly simulates the mixing layer in the spatial domain.

The dynamics following the prescription of this superposed wave spectrum at the inflow boundary leads to an interesting development of the layer where three rolled up vortices corresponding to the fundamental merge together, instead of two vortex structures pairing at a time. This collective interaction leads to a larger growth rate of the layer compared with the baseline case, as shown in Fig. 9. Corresponding spatially growing passive scalar and vorticity contours are shown in Figs. 10 and 11, respectively. It is shown clearly through these two contour plots that three rolled up structures coalesce together to form a bigger structure, thus leading to higher growth rate of the layer. This phenomenon was observed by Ho and Huang[19] in their experiment. For a comparison, passive scalar and vorticity contour plots corresponding to the baseline DNS of spatialy growing layer case are shown in Figs. 12 and 13.

2.2 Mixing Layer with a Velocity Ratio, r= 0.28

The results presented so far correspond to a velocity ratio of 0.5. Next, a velocity ratio of 0.28 was chosen to make some initial comparison with the experiment of Ely and Little[30,31]. Other studies around velocity ratio of approximately 0.28, notably[24,32], were carried out earlier. The influence of velocity ratio on the growth rate of a mixing layer was observed to be significant[33].

In the present case, a fundamental and its first subharmonic were considered that lead to one pairing, since that corresponds to experimental conditions[30,31]. Four different forcing levels were chosen, as shown in the momentum thickness plot in Fig. 14(a). The axes of the DNS results are scaled to match the location of the first pairing as observed in the experiment. After the initial linear development, the slope of the θ-x curve is about 0.03, in approximate agreement with the experiment for actuation conditions, as shown in Fig. 14(b). It is noted here that the experiment has been conducted with the actuation imposed at a location near the origin which is not the same location as the origin of the free shear layer corresponding to the DNS. So we should not expect an exact quantitative agreement, only the trends should agree. As expected, higher forcing levels lead to higher growth rates, although the growth rate is not significantly affected as in the case of lower velocity ratio, as shown earlier. The growth rate given by the experimental baseline conditions tends to be smaller than the DNS results. That is expected since the forcing levels of imposed perturbations with DNS are higher than those present in the unforced layer in the experiment. An interesting observation made here is that the growth rate of the layer given by the average slope of the $\theta - x$ curve shown in red in Fig. 14(a) is in inverse proportion to that for the velocity ratio of 0.5, as shown in Fig. 3(a). Similar trend in the maximum growth rates was also found in an earlier study[33] that the growth rate increases proportionally to the velocity ratio.

Fig. 14(b) shows a direct comparison between the experiment[30,31] and the DNS results. As pointed out earlier, higher forcing levels were used in the experiment. So we should expect some mismatch between DNS and experiment. At the location, x = 450 mm, first pairing was observed in the experiment. This fact was used to scale the DNS results for comparison with the experiment. The slope of the DNS curve after x=300 mm is about the same as that shown by experimental data for actuation conditions. More detailed comparisons with the experiment[30,31] and DNS will be made in a forthcoming paper. In the initial development of the momentum thickness profiles predicted by the DNS, we observe a linear growth indicated by the exponential growth of the profiles, which is not observed in the experiment. The reason for this is that the actuation in the experiment is applied at higher levels so that the linear development is bypassed.

2.3 PID Control

Results corresponding to the PID control are shown in Fig. 15(a,b). Fig 15(a) shows how the target shear layer thickness is iteratively reached within a given number of iterations, beginning with an arbitrarily picked initial state. The control parameter is the amplitude of the fundamental wave length with a fixed ratio between the amplitudes of the subharmonics and the fundamental. The target state, shown in red symbols, is matched almost exactly by the converged (final) state shown in yellow. The initial state is shown in black. The resulting amplitude convergence history is shown in Fig. 15(b), where after a given number of iterations, as the amplitude changes with each iteration (shown along the abscissa) , the error shown along

the ordinate monotonically reaches sufficiently close to zero. The converged value of the amplitude of the fundamental is shown to reach the desired value.

3 Concluding Remarks

Perturbations of different frequencies with given amplitude and phase were imposed on a diffused tangential velocity discontinuity in the temporal domain. The subsequent development of the mixing layer was tracked through the momentum and visual thickness plots. Some quantitative information was obtained, especially with respect to the role of the first subharmonic of the fundamental wave. The relative effects of the unstable modes on the development of the mixing layer was measured computationally. A subset of these perturbation sets was also imposed near the origin of the mixing layer and DNS of the layer was carried out directly in the spatial domain. Differences between the baseline and collective interaction cases were highlighted. The collective interaction leads to a higher growth rate of the spatially growing layer compared with the binomial interaction (pairing). PID control of a baseline binomial case was demonstrated with the amplitude control as the control parameter.

4 References

[1]Kaul, U. K., "Efficient CFD-Based PID Control of Free Shear Layer Flow," AIAA 2013-2986, June 2013

[2]Roshko, A., "Modeling: Present and Future, Whither Turbulence? Turbulence at the Crossroads," Lecture Notes in Physics, Springer, 357, 1990, pp 486-489

[3]Cordier, L., Noack, B. R., Tissot, G., Lehnasch, G., Delville, J., Balajewicz, M., Daviller, G., Niven, R. K., "Identification strategies for model-based control," Exp Fluids (2013) 54:1580, DOI 10.1007s00348-013-1580-9

[4]Paschereit, C. O., Gutmark, E. and Weisenstein, W., "Suppression of Combustion Instabilities by Acoustic Control of Shear Layer Properties," Advances in Turbulence VII, Fluid Mechanics and Its Applications, Volume 46, 1998, pp 293-296.

[5]Pandey, K. M. and Sivasakthivel, T., "CFD Analysis of Mixing and Combustion of a Scramjet Combustor with a Planer Strut Injector," Int. Journal of Enviromental Science and Development, Vol. 2, No. 2, April 2011

[6]C.C.L. Yuan, Krstic, M., and Bewley, T. R., "Active control of jet mixing," IEE Proc.-Control Theory Appl., Vol. 151, No. 6, November 2004

[7]Wei, M. and Freund, J. B., "A noise-controlled free shear flow," J.Fluid Mech., vol. 546, pp. 123-152, 2006

[8]Rumsey, C. L., "Successes and Challenges for Flow Control Simulations (Invited)," AIAA-2008-4311, 4th AIAA Flow Control Conference, June 23-26, 2008, Seattle, WA

[9]Cattafesta, L. and Williams, D., Rowley, C. and Farrukh, A., "Review of Active Control of Flow-Induced Cavity Resonance," AIAA 2003-3567

[10]Williams, D. R. and Rowley, C. W., "Recent Progress in Closed-Loop Control of Cavity Tones," AIAA 2006-0712, 14th AIAA Aerospace Sciences Meeting, Jan. 2006

[11]Rowley, C. W., Williams, D. R., Colonius, T., Murray, R. M. and MacMynowski, D. G., "Linear models for control of cavity flow oscillations," J. Fluid Mech., vol. 547, pp. 317-330, 2006

[12]Cattafesta III, L. N., Song, Q., Williams, D. R., Rowley, C. W., and Alvi, F. S., "Active Control of Flow-Induced Cavity Oscillations," Progress in Aerospace Sciences, Vol. 44 (2008) pp. 479-502.

[13]Rowley, C. W., and Williams, D. R., "Dynamics and Control of High-Reynolds-Number Flow over Open Cavities," Annual Review of Fluid Mechanics, Vol. 38 (2006) (article by invitation).

[14]Bernardini, C., Benton, S. I., Chen, J-P. and Bons, J. P., "Exploitation of Subharmonics for Separated Shear Layer Control on a High-Lift Low-Pressure Turbine Using Acoustic Forcing," J. Turbomachinery, Vol. 136, Issue 5, October 2013

[15]Pastoor, M., Henning, L., Noack, B. R., King, R. and Tadmor, G., "Feedback shear layer control for bluff body drag reduction," J. Fluid Mech., vol. 608, pp. 161-196, 2008

[16]Pastoor, M., King, R., Noack, B. R. and Tadmor, G., "Observers and Feedback Control for Shear Layer Vortices," Paper MoA15.3, Proc. of the 44th IEEE Conference on Decision and Control and the European Control Conference 2005, Seville, Spain, December 12-15, 2005

[17]Kaul, U. K., "Do large structures control their own growth in a mixing layer ? An assessment", J. Fluid Mech., vol. 190, pp. 427-450, 1988

[18]Kaul, U. K., "On Some Aspects of Wave Interactions in Plane Mixing Layers," Wave Phenomena, Theoretical, Computational and Practical Aspects, Eds. Lui Lam and Hedley C. Morris, Springer-Verlag, 1988

[19]Ho, C. and Huang, L-S, "Subharmonics and vortex merging in mixing layers," J. Fluid Mech., vol. 119, 1982, pp. 443-473

[20]Oster, O. and Wygnanski and I., "The forced mixing layer between parallel streams," J. Fluid Mech., vol. 123, 1982, pp. 91-130

[21]Bell, J. H. and Mehta, R. D., "Development of a Two-Stream Mixing Layer from Tripped and Untripped Boundary Layers," AIAA J., vol. 28, no. 12, Dec. 1990, pp. 2034-2042.

[22]Delville, J., Bellin, S., Garem, J. H., and Bonnet J. P., "Analysis of Structures in a Turbulent, Plane Mixing Layer by Use of a Pseudo Flow Visualization Method Based on Hot-Wire Anemometry," Advances in Turbulence 2, eds: H.-H. Fernholz and H. E. Fiedler, Proceedings of the Second European Turbulence Conference, Berlin, Aug 30-Sept 2, 1988, Springer Verlag, Berlin, 1989, pp. 251-256.

[23] Delville, J., "Plane turbulent mixing layer from C.E.A.T. Poitiers," CEAT/LEA UMR CNRS 6609, Poitiers Cedex, France

[24]Winant, C. D. and Browand, F. K., "Vortex pairing : the mechanism of turbulent mixing layer growth at moderate Reynolds number," J . Fluid Mech. (1974), vol. 63, part 2, pp. 237-255

[25]Betchov, R. and Criminale, W. O., Jr., Stability of Parallel Flows, Academic Press, New York, London, 1967

[26]Zohar, Y. and Ho, C-M, "Dissipation scale and control of fine-scale turbulence in a plane mixing layer," J. Fluid Mech. (1996), vol. 320, pp 139-161.

[27]Kaul, U. K., "EDLFLOW-F: A Next-Generation High-Order High-Fidelity All-Speed Time-Accurate Flow Solver for Simulating Fluid Flows," NASA Invention Disclosure, NASA-ARC-16349-1, 2009; also AIAA J., vol. 51, no. 6, June 2013, pp. 1516-1521

[28]Lele, S., “Compact finite difference schemes with spectral-like resolution," J. Comput. Phys., Vol. 103 1992, pp. 16-42.

[29]Gaitonde, D. V., Shang, J. S. and Young, J. L., “Practical aspects of high-order accurate finite-volume schemes for electrodynamics," AIAA Paper 97-0363, 35th AIAA Aerospace Sciences Meeting Exhibit, Reno, NV, Jan. 6-9, 1997; Int. J. Numer. Meth. Eng. 45, 1999, pp. 1849.

[30]Ely, R. and Little,J.,“Mixing Layer Excitation by Dielectric Barrier Discharge Plasma Actuators," AIAA Paper 2013-1012, 51st AIAA Aerospace Sciences Meeting, Jan. 7 - 10, 2013, Grapevine, Texas

[31]Ely, R. and Little, J., “The Mixing Layer Perturbed by Dielectric Barrier Discharge," AIAA 2013-2753, June 2013

[32]Brown, G. L. and Roshko, A., “On density effects and large structure in turbulent mixing layers," J. Fluid Mech. (1974), vol. 64, part 4, pp. 775-816.

[33]Monkewitz, P. A. and Huerre, P., “Influence of the velocity ratio on the spatial instability of mixing layers," Phys. Fluids, vol. 25, 1982, pp 1137-1143

5 Figures

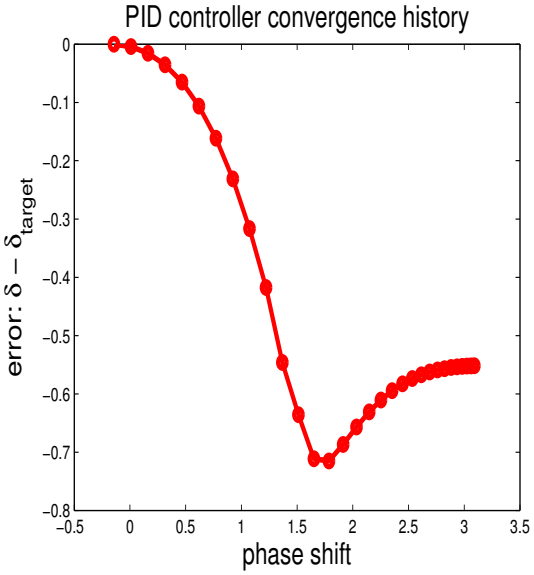

Figure 1: Phase control of the mixing layer; taken from Ref. 1. Iterates proceed from right to left and are represented by the symbols.

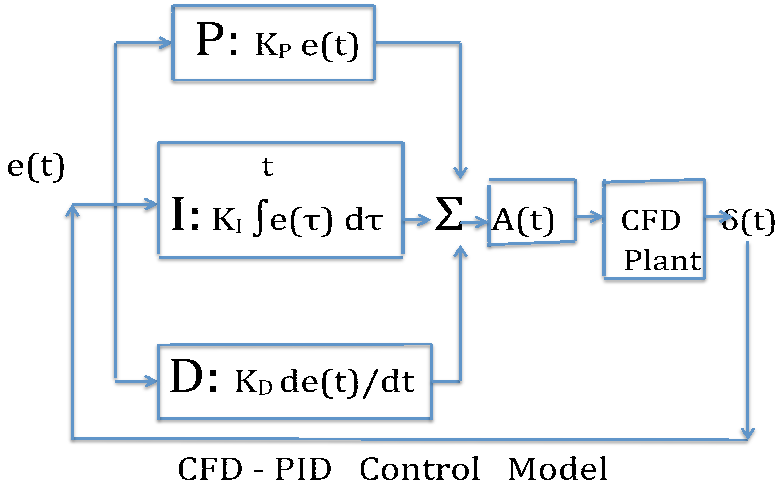

Figure 2: PID block diagram: amplitude control of the mixing layer thickness; $e(t) = |\delta(t) - \delta_{target}|$.

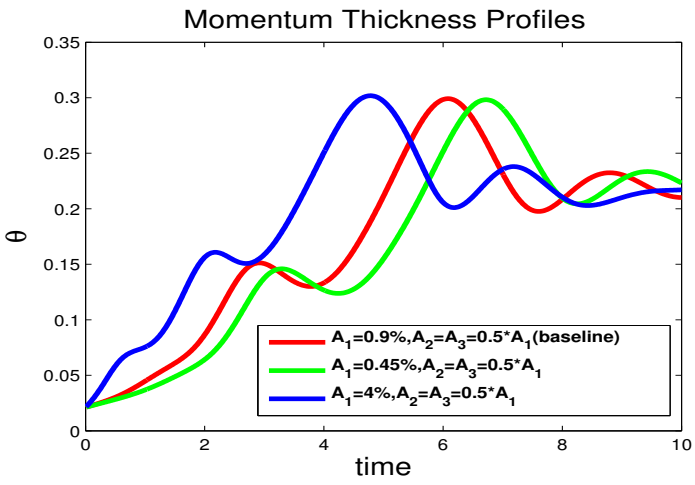

(a) Momentum thickness

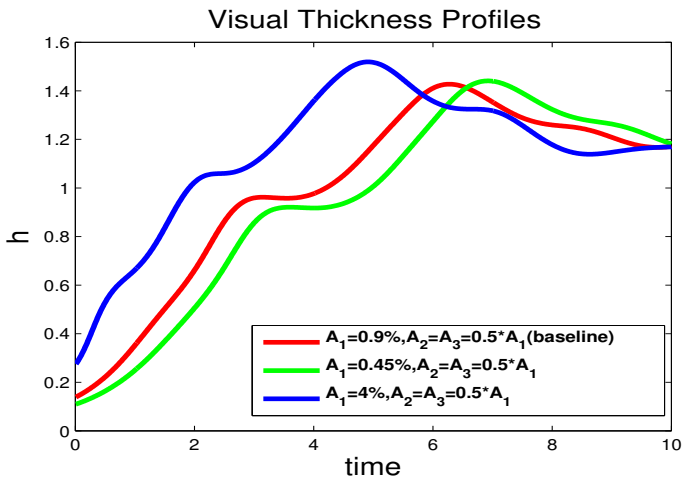

(b) Visual (streamline) thickness

Figure 3: Thickness profiles: baseline case (zero phase shift) with imposed perturbations in the linear range. A_1, A_2 and A_3 are the amplitudes of the fundamental, first and third subharmonics.

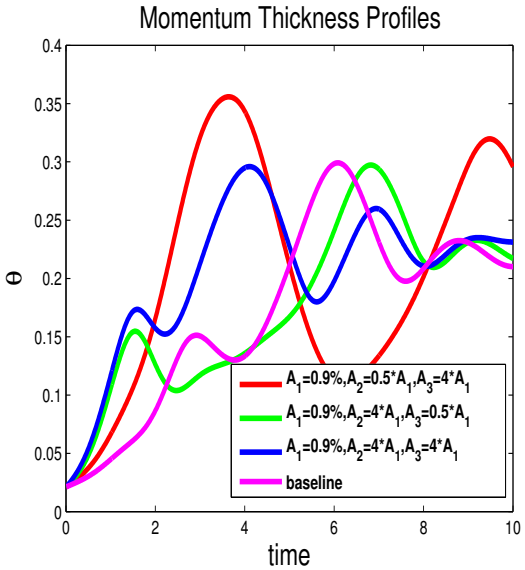

(a) Momentum thickness

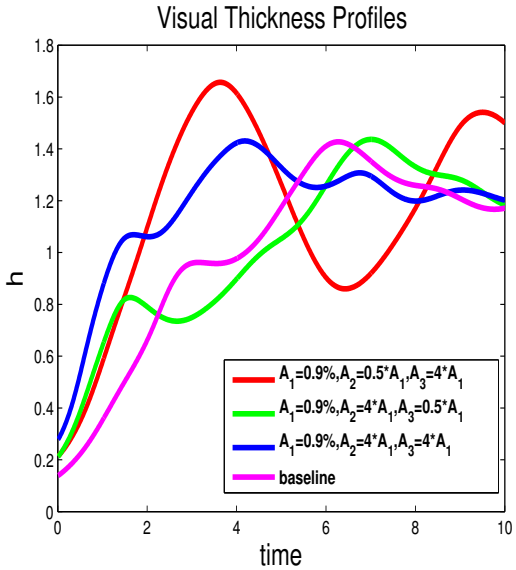

(b) Visual thickness

Figure 4: Thickness profiles: relative comparison of fundamental, its first and third subharmonic.

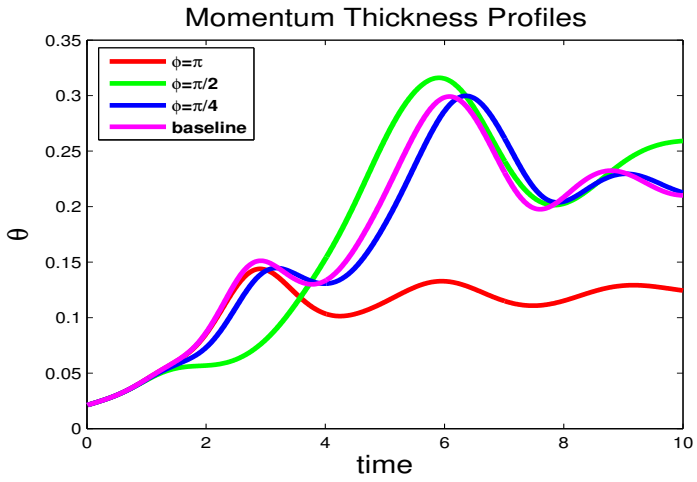

Figure 5: Momentum thickness profiles: role of phase shift among fundamental, its first and third subharmonics.

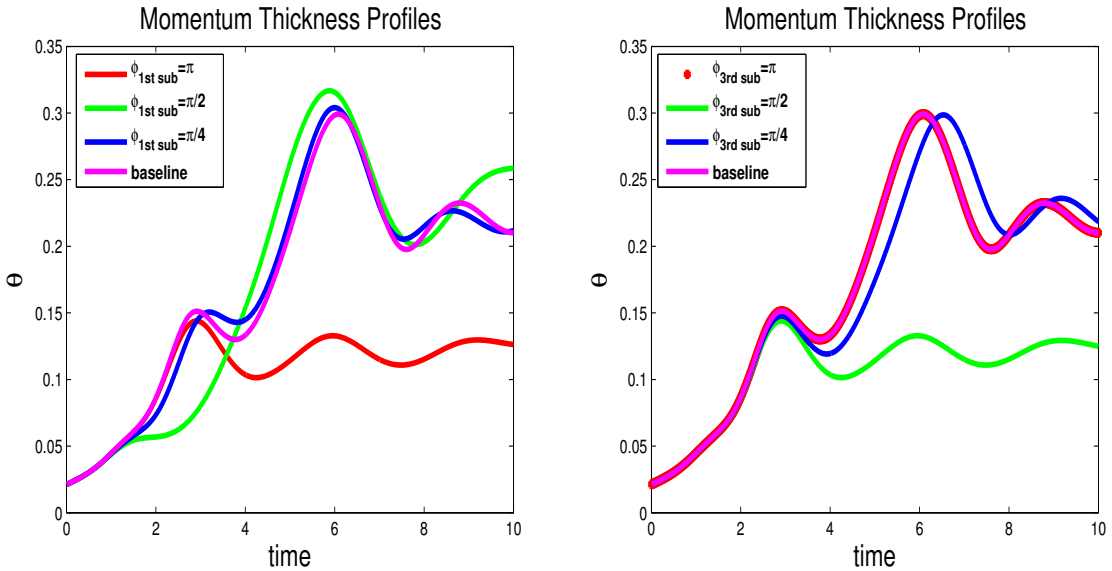

(a) fundamental and 2nd subharmonic (b) fundamental and 3rd subharmonic

Figure 6: Momentum thickness profiles: selective phase shifts between harmonics.

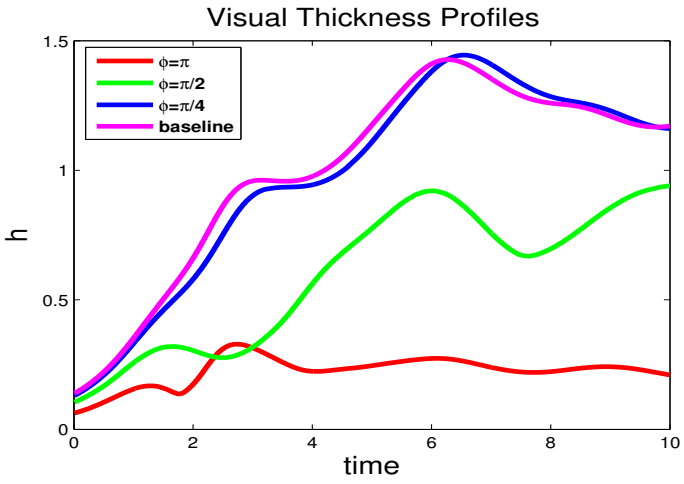

Figure 7: Visual thickness profiles: role of phase shift among fundamental, its first and third subharmonics.

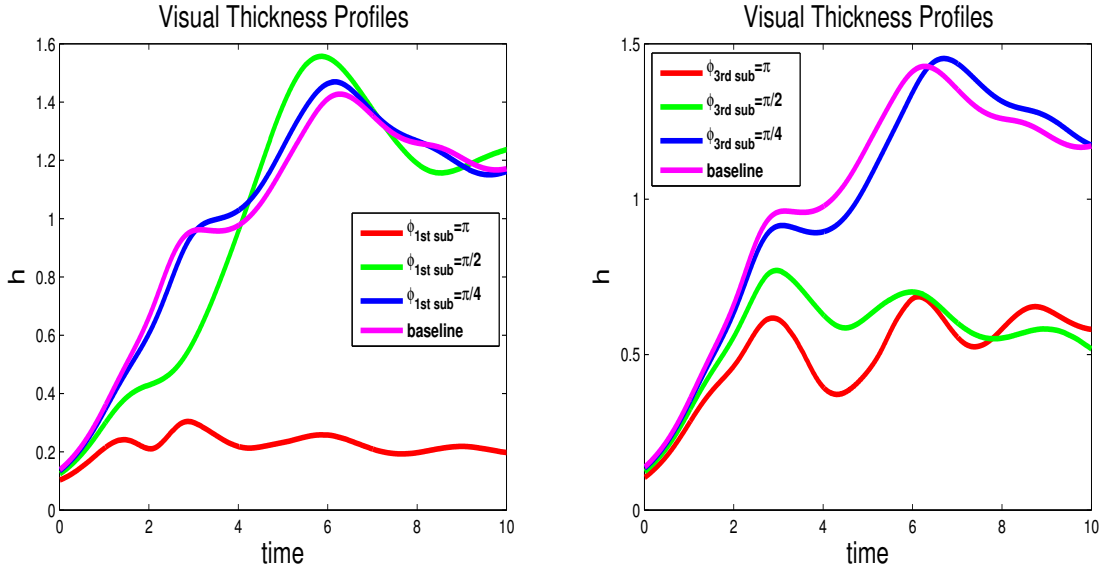

(a) fundamental and 2nd subharmonic (b) fundamental and 3rd subharmonic

Figure 8: Visual thickness profiles: selective phase shift between harmonics.

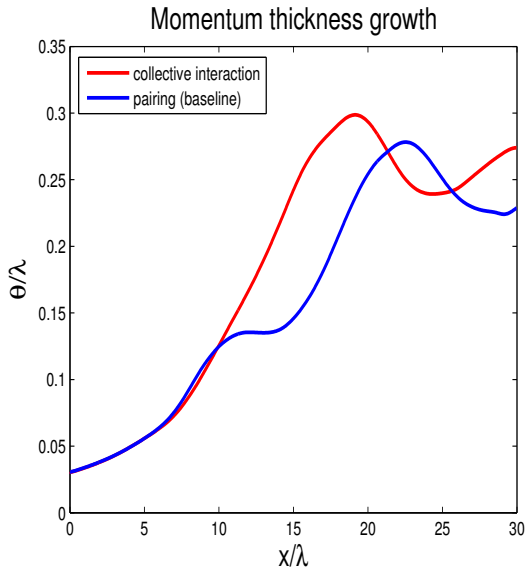

Figure 9: Momentum thickness profiles: a comparison of collective coalescence with baseline pairing

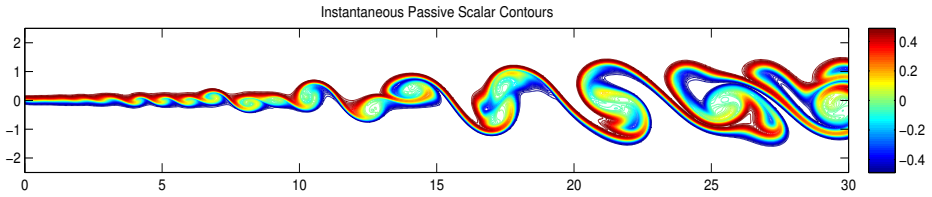

Figure 10: Passive scalar contours showing collective interaction, calculated using spatially developing simulation (EDLFLOW).

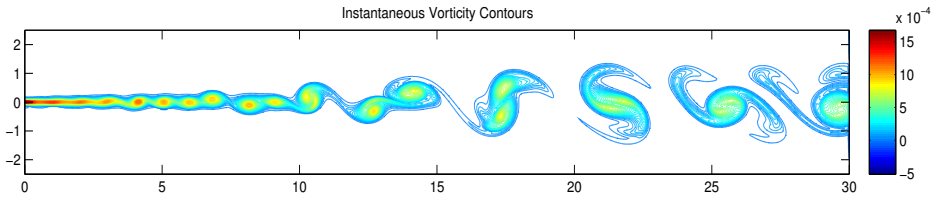

Figure 11: Vorticity contours showing collective interaction, calculated using spatially developing simulation (EDLFLOW).

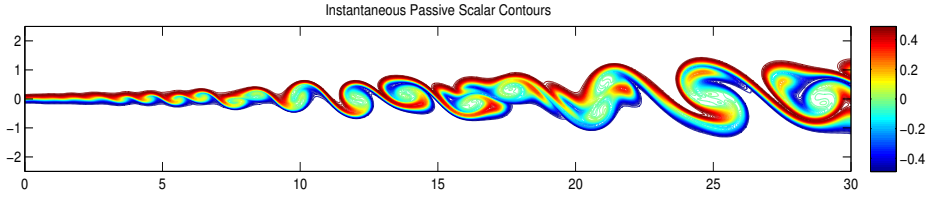

Figure 12: Passive scalar contours showing pairing, calculated using spatially developing simulation (EDLFLOW).

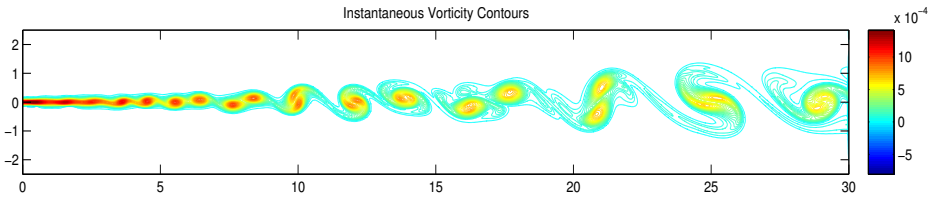

Figure 13: Vorticity contours showing pairing, calculated using spatially developing simulation (EDLFLOW).

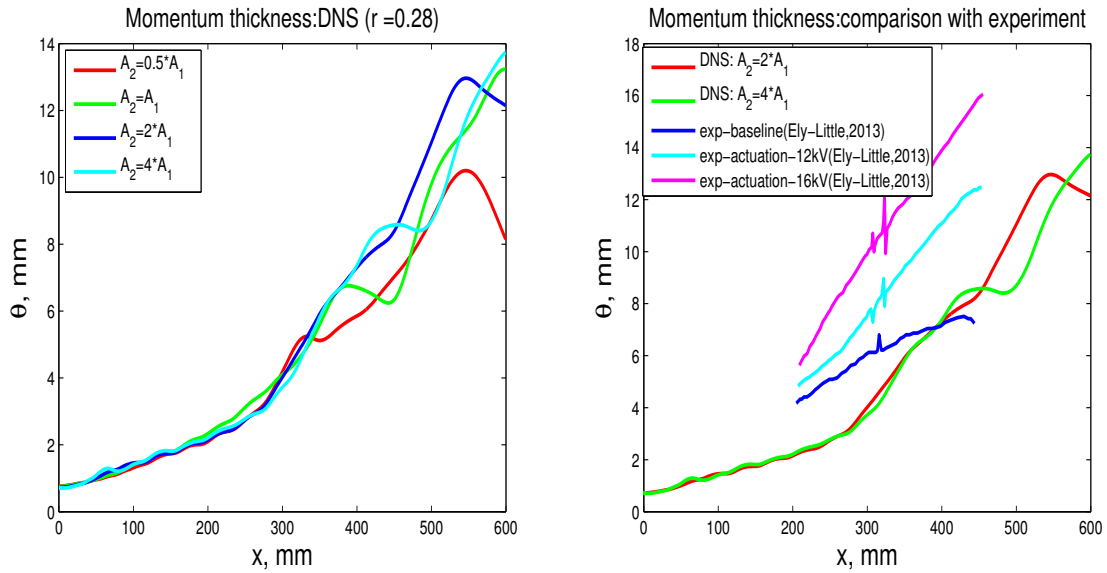

(a) DNS results (b) DNS comparison with experiment

Figure 14: Momentum thickness profiles: effect of forcing levels on fundamental and the first subharmonic, r = 0.28

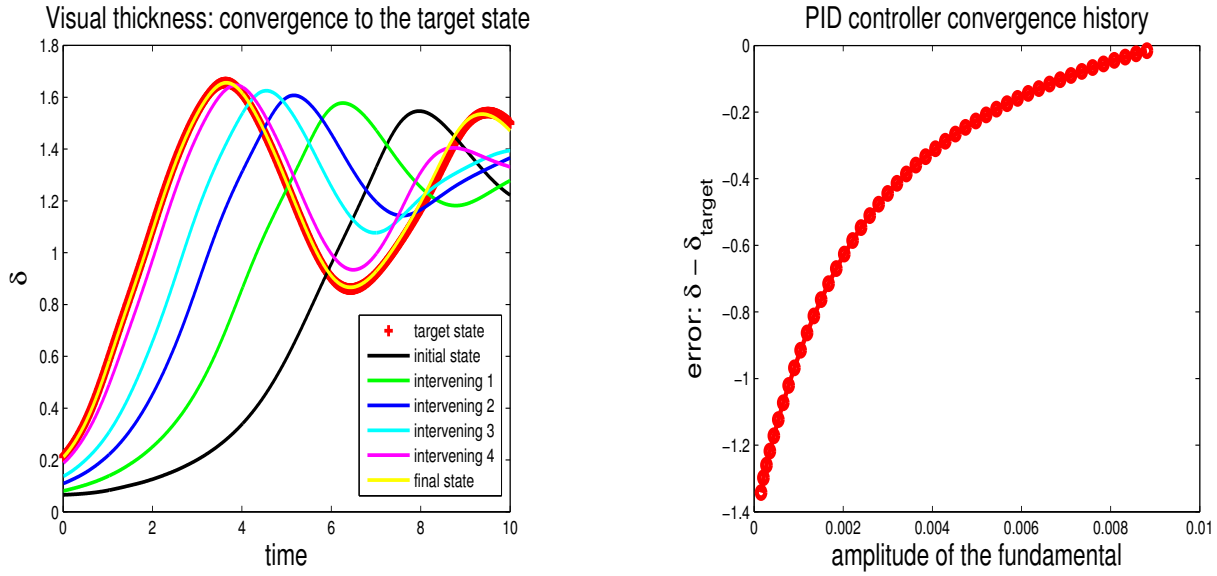

(a) Visual thickness (b) convergence of amplitude

Figure 15: PID Iteratioons leading to the target state